Exocytosis-Mediated Urinary Full-Length Megalin Excretion Is Linked With the Pathogenesis of Diabetic Nephropathy

Shankhajit De,[1,2] Shoji Kuwahara,[2] Michihiro Hosojima,[3] Tomomi Ishikawa,[1] Ryohei Kaseda,[1] Piyali Sarkar,[1,2] Yusuke Yoshioka,[4] Hideyuki Kabasawa,[3] Tomomichi Iida,[1] Sawako Goto,[1] Koji Toba,[1] Yuki Higuchi,[1] Yoshiki Suzuki,[5] Masanori Hara,[6] Hiroyuki Kurosawa,[7] Ichiei Narita,[1] Yoshiaki Hirayama,[7] Takahiro Ochiya,[4] and Akihiko Saito[2]

Diabetes 2017;66:1391–1404 | DOI: 10.2337/db16-1031

Efficient biomarkers for diabetic nephropathy (DN) have not been established. Using ELISA, we found previously that urinary levels of full-length megalin (C-megalin), a multiligand endocytic receptor in proximal tubules, was positively correlated with DN progression in patients with type 2 diabetes mellitus (T2DM). Here, we found that urinary extracellular vesicle (UEV) excretion and C-megalin content in UEVs or in their exosomal fraction increased along with the progression of the albuminuric stages in patients with T2DM. Cultured immortalized rat proximal tubule cells (IRPTCs) treated with fatty acid–free BSA or advanced glycation end product–modified BSA (AGE-BSA), endocytic ligands of megalin, increased EV excretion, and their C-megalin content. C-megalin excretion from IRPTCs via extracellular vesicles was significantly blocked by an exosome-specific inhibitor, GW4869, indicating that this excretion is mainly exocytosis-mediated. AGE-BSA treatment of IRPTCs caused apparent lysosomal dysfunction, which stimulated multivesicular body formation, resulting in increased exosomal C-megalin excretion. In a high-fat diet–induced, megalin-mediated kidney injury model in mice, urinary C-megalin excretion also increased via UEVs. Collectively, exocytosis-mediated urinary C-megalin excretion is associated with the development and progression of DN in patients with T2DM, particularly due to megalin-mediated lysosomal dysfunction in proximal tubules, and hence it could be a candidate biomarker linked with DN pathogenesis.

Diabetic nephropathy (DN) is the leading cause of end-stage renal disease (1) and increases morbidity and mortality in patients with type 2 diabetes mellitus (T2DM) (2). Phenotypic changes in proximal tubule epithelial cells (PTECs) are the initial signs of DN (3), and the consequent tubulointerstitial damage plays a crucial role in the progression to end-stage renal disease (4). Albuminuria has been used as a conventional biomarker for DN, but its clinical relevance as a surrogate marker has been controversial (5). Thus, efficient biomarkers associated with the development and progression of DN have not been established.

Megalin, a large (~600 kDa) glycoprotein member of the LDL receptor family (6), plays a pivotal role in the endocytosis of diverse glomerular-filtered substances into PTECs (7,8). We have recently established that megalin mediates autolysosomal dysfunction in PTECs by taking up pathogenic ligands, leading to the development of tubuloglomerular alterations in a high-fat diet (HFD)–induced diabetes model (9). Advanced glycation end products (AGEs) are also filtered by glomeruli and reabsorbed by PTECs, causing glycotoxicity (10), and megalin is involved in the uptake of

[1]Division of Clinical Nephrology and Rheumatology, Niigata University Graduate School of Medical and Dental Sciences, Chuo-ku, Niigata, Niigata, Japan
[2]Department of Applied Molecular Medicine, Niigata University Graduate School of Medical and Dental Sciences, Chuo-ku, Niigata, Niigata, Japan
[3]Department of Clinical Nutrition Science, Niigata University Graduate School of Medical and Dental Sciences, Chuo-ku, Niigata, Niigata, Japan
[4]Division of Molecular and Cellular Medicine, National Cancer Center Research Institute, Chuo-ku, Tokyo, Japan
[5]Health Administration Center, Niigata University, Nishi-ku, Niigata, Niigata, Japan
[6]Department of Pediatrics, Yoshida Hospital, Tsubame, Niigata, Japan
[7]Diagnostics Research Department, Life Innovation Research Institute, DENKA Innovation Center, Denka Co., Ltd., Machida, Tokyo, Japan
Corresponding author: Akihiko Saito, akisaito@med.niigata-u.ac.jp.

Received 24 August 2016 and accepted 15 February 2017.
This article contains Supplementary Data online at http://diabetes.diabetesjournals.org/lookup/suppl/doi:10.2337/db16-1031/-/DC1.

filtrated AGEs by PTECs (11). Previously, we established a sandwich ELISA to measure the ectodomain (A-megalin) and full-length (C-megalin) forms of urinary megalin using specific monoclonal antibodies against the amino-terminal and carboxy-terminal of megalin, respectively. Compared with normal control subjects (NCs), urinary C-megalin excretion levels in T2DM patients were found to be elevated and positively correlated with the development and progression of DN (12). In addition, in our recent longitudinal analysis of normoalbuminuric patients with T2DM, measurement of urinary C-megalin was found to be useful for predicting the early progression of DN (T.Ii., M.Ho., H.Ka, A.S., unpublished data). However, the molecular mechanism of urinary C-megalin excretion is not understood clearly, although it is known to be excreted in association with extracellular vesicles (EVs) (12).

EVs are nano-sized membrane vesicles (30–2,000 nm in diameter) that include mainly exosomes, microvesicles, and apoptotic bodies, which are either excreted by exocytosis or direct budding and blebbing of plasma membranes into extracellular spaces (13,14). Exosomes (30–130 nm) are excreted from almost all types of cell upon fusion of multivesicular bodies (MVBs) with cell membranes, and these are being studied extensively for the discovery of potential biomarkers in different diseases (15).

Hence, here we studied urinary EVs (UEVs) in connection with their C-megalin content and PTEC injury during the progression of DN.

RESEARCH DESIGN AND METHODS

Collection of UEVs

Fresh second urine samples were collected from adult outpatients with T2DM (n = 56) at Niigata University Medical and Dental Hospital from 2013 to 2016 and from NC volunteers (n = 19) who participated in public medical examinations at Co-op Chemicals Co., Ltd. (Niigata, Japan) from 2014 to 2016, with written informed consent, based on the approval of the ethics committee of Niigata University, performed in accordance with the principles embodied in the Declaration of Helsinki. UEVs were collected from protease inhibitor–treated urine samples (16). As described previously (12,16), the urine samples were centrifuged at 17,000g for 15 min at 4°C, followed by high-speed centrifugation of the supernatant at 200,000g for 1 h at 4°C using a P40ST rotor and Himac CP-80β ultracentrifuge (Hitachi-Koki Co., Ltd.). UEVs in the second pellet were lysed or suspended in PBS, depending on the purpose, and standardized by creatinine levels that were measured using an enzymatic method. The protein concentration of EVs was determined by a bicinchoninic acid protein assay (Pierce). Physical examination and blood test data of T2DM patients were collected during the same visit as their urine samples and those of NCs were obtained <1 year before urine collection. The albumin-to-creatinine ratio (ACR; in milligrams per gram) was determined using the collected urine samples.

Transmission Electron Microscopy

For observation of UEVs, the urinary second pellet was suspended in PBS, applied to a carbon-coated 200-mesh copper grid (Nisshin EM Co., Ltd.), fixed with 4% paraformaldehyde phosphate buffer solution (Gibco) for 10 min, washed with distilled water, contrasted with 2% uranyl acetate (Wako) for 10 min, and visualized under a JEOL 1400 Transmission Electron Microscope (JEOL USA, Inc.) at different magnifications at 100 KV. For EV-bound beads, the pellet was fixed in a mixture of 4% paraformaldehyde, 0.1% glutaraldehyde in cacodylate-HCl (Sigma-Aldrich) buffer at pH 7.2 for 45 min and postfixed with 1% osmium tetroxide (Sigma-Aldrich) for 1 h. Subsequently, it was dehydrated in an ethanol series, treated with 400 μL propylene oxide (Sigma-Aldrich), and exposed to 50% epoxy resin (epon; Polysciences, Inc.) for 30 min and to 75% resin for 1 h at room temperature. Further, it was exposed to 100% resin and dried in an oven. The pellet was sliced into ultrathin sections (80 nm thick), treated with tannic acid, and stained with lead acetate.

Nanoparticle Tracking Analysis

Nanoparticle tracking analysis (NTA) was performed using a NanoSight LM10 instrument (NanoSight Ltd.) equipped with NTA 2.3 software 3.0 at a particle concentration within the optimal working range of the system (17). EVs were collected from creatinine-standardized urine and from culture media as described above. Size distributions are presented as the mean and SEM of three video recordings per sample.

Immunoelectron Microscopy

The diluted EV fraction was fixed on a copper grid as described above and then blocked using 0.05 mol/L glycine/PBS and 1% BSA/PBS, respectively, for 10 min each. The grid was rewashed and incubated overnight with a primary antibody diluted in 0.02% Triton X-100 in PBS. The grid was washed with PBS and incubated with 5 nm gold-conjugated anti-mouse IgG antibody G7527 (1:25; Sigma-Aldrich) for 60 min at room temperature. The grid was washed again, fixed with 2.5% glutaraldehyde for 5 min, washed once more, and embedded with 0.5% uranyl acetate (18). The primary antibodies and their dilutions were as follows: mouse monoclonal anti-megalin antibody C-25 (22.2 μg/mL, final concentration) (12), mouse monoclonal anti-CD81 antibody sc-7637 (1:50; Santa Cruz Biotechnology), and mouse monoclonal anti-podocalyxin antibody 22A4 (15 μg/mL, final concentration) (19).

Immunoblotting

Immunoblotting was carried out as described previously (9). The primary and secondary antibodies and their dilutions are mentioned in the Supplementary Data.

Purification of Exosome-Enriched UEVs

Exosome-enriched UEVs were purified from the total population of UEVs using a human CD63 or CD81 isolation/detection kit (Invitrogen) according to the

manufacturer instructions. After purification, the beads were either processed for transmission electron microscopy (TEM) as described above or lysed by adding 2× sample buffer for immunoblot analysis. For comparative analysis of C-megalin content in exosomes, we prepared the total UEVs from NCs (n = 11) and T2DM patients (n = 33), and suspended in variable volumes of PBS, depending on their urinary creatinine levels. Exosomes were purified from the same volume of those UEV samples using an excess amount of anti-CD81 antibody-coated paramagnetic beads, and the beads were lysed by adding the same volume of 2× sample buffer, the same volume of samples was loaded in each well of an SDS-PAGE gel, and immunoblotting was performed against C-megalin and tumor susceptibility gene 101 (TSG101).

Purification and Analysis of C-Megalin–Containing UEVs

C-megalin–containing UEVs were purified using recombinant rat receptor–associated protein (RAP), a high-affinity Ca^{2+}-dependent ligand of megalin (20), which was prepared using a prokaryotic expression system as a fusion protein with glutathione S-transferase (GST), as described previously (20). The specificity of RAP binding to megalin in UEVs was verified by ligand blotting analysis, as described previously (21), using GST-RAP as a ligand of megalin, which was further detected using an anti-GST antibody. For purification of C-megalin–containing UEVs, glutathione Sepharose 4B beads (Amersham Bioscience) were incubated with recombinant GST-RAP or GST in the presence of 1 mmol dithiothreitol for 1 h at room temperature. The beads coated with the recombinant proteins were incubated with UEVs in the presence of binding buffer containing 10 mmol HEPES and 150 mmol NaCl with or without Ca^{2+} overnight at 4°C. The next day, the beads were collected and washed with the respective binding buffer and used for further experiments.

MicroRNA and mRNA Quantification

Total RNA was isolated from GST-RAP–captured UEVs and cultured cells using a Total Exosome RNA and Protein Isolation Kit (ThermoFisher Scientific) and GenElute Mammalian Total RNA Miniprep Kit (Sigma-Aldrich), respectively. MicroRNA (miRNA)-192 and miRNA-16 were both quantified using a TaqMan MicroRNA Assay (Applied Biosystems), and their relative quantities were calculated with the $2^{-\Delta\Delta Ct}$ method (22) using the normalization control RNA RNU6. See the Supplementary Data for further details.

Preparation of AGE-BSA

AGE-BSA was prepared with a modified method that has been described previously (23). Briefly, fatty acid–free (FAF)-BSA (Calbiochem) (200 μg/mL in PBS) was treated with 33 mmol/L methylglyoxal (Sigma-Aldrich), incubated at 37°C for 7 days, dialyzed three times with PBS, and filtered through a 0.2-μm filter.

Cell Culture and EV Collection From Culture Media

We cultured immortalized rat proximal tubule cells (IRPTCs) (a gift from Professor Julie R. Ingelfinger, Massachusetts General Hospital, Boston, MA) as described previously (9). The cells were allowed to grow for 24 h; were serum starved for 12 h; and were incubated with PBS (vehicle), FAF-BSA (1 mg/mL, final concentration), or AGE-BSA (1 mg/mL) for 48 h. Then, culture media were collected, and EVs excreted by the cells were isolated using a differential ultracentrifugation method optimized for cultured cells (24). The exosome excretion inhibitor GW4869 (4 μmol/L; Sigma-Aldrich) and lysosome inhibitors bafilomycin A1 (50 nmol/L; Sigma-Aldrich) and chloroquine phosphate (50 μmol/L; Wako) were also used for experiments with the cells.

Assays for Lysosomes in Cultured IRPTCs

IRPTCs were cultured in the medium described above. Subsequently, the cells were starved for 12 h and treated for 24 h with the substances described above. The cells were stained with LysoTracker Deep Red (Life Technologies) and NucBlue Live Cell Stain (Life Technologies), as described previously (9). LysoTracker Deep Red–positive vacuoles and cell surface area were evaluated using Image-Pro Plus version 7.0 in 20 cells selected randomly for each condition.

Induction of HFD-Induced Diabetes Model in Mice, Followed by UEV and Urinary C-Megalin Excretion Analysis

C57BL/6J mice (n = 12) were fed an HFD (60% of total calories from fat; Research Diets) by paired feeding with those (n = 12) fed a normal-fat diet (NFD) (10% of total calories from fat; Research Diets) from 11 weeks of age for 4 weeks. Urine was collected for 72 h in metabolic balance cages, after which it was used for collecting UEVs by the ultracentrifugation method described above. Briefly, collected urine samples were subjected to ultracentrifugation at 17,000g twice and then at 100,000g for 60 min. The resulting pellets were suspended in PBS and used for NTA as described above. Also, urine samples were collected for 24 h, and UEVs were prepared from urine collected for 48 h from mice fed an HFD or NFD for 6 weeks were used for immunoblotting using anti-megalin C-25 antibody as described above after urinary volume standardization.

Statistical Analysis

The data were analyzed by one-way ANOVA followed by Bonferroni and Tukey multiple-comparisons tests using GraphPad Prism statistical software version 5 (GraphPad Software, Inc.) and SPSS statistical software version 22 (SPSS, Inc.). The level of significance was $P < 0.05$. For animal studies, comparisons between two groups were made by Student t test (two-tailed). For single-regression analysis, Spearman rank correlation tests were performed using SPSS statistical software version 22 (SPSS, Inc.).

RESULTS

Patients With T2DM Excrete a Greater Number of UEVs Than NCs

We collected urine from NCs (n = 19) and patients with T2DM (n = 56) at different albuminuric stages who were classified into the following three groups depending on their ACR: normoalbuminuric T2DM (Nor-DM) with

ACR <30 mg/g (n = 20); microalbuminuric T2DM (Mi-DM) with ACR ≥30 and <300 mg/g (n = 17); and macroalbuminuric T2DM (Ma-DM) with ACR ≥300 mg/g (n = 19). UEVs were collected using the classic differential centrifugation method (12,16). The NC criteria and clinical parameters of the NCs and T2DM patients are shown in Supplementary Tables 1 and 2, respectively.

In the differential centrifugation method, UEVs are expected to be enriched in the urinary second pellet. To characterize the UEVs, we visualized the second pellet by TEM (Supplementary Fig. 1*A*) and investigated their frequency distribution by NTA using NanoSight (Supplementary Fig. 1*B*). NanoSight analysis confirmed that the second pellet was exosome enriched, as the mode size of UEVs (113 nm) was within the size range of exosomes (15). Immunoelectron microscopy against the exosomal marker CD81 (25) (Supplementary Fig. 1*C*) and immunoblot analysis against exosomal markers, such as CD81, apoptosis-linked gene 2–interacting protein X (Alix) (26), and TSG101 (26) further confirmed the presence of exosomes in the second pellet and their scarcity in the first pellet (Supplementary Fig. 1*D*). Further, NTA revealed a positively correlated increase in the total number of UEVs in creatinine-standardized urine samples of T2DM patients with the development and progression of DN (Fig. 1*A*). Because of the lack of a comprehensive size range of different kinds of UEVs, we considered the smaller UEVs (<130 nm in diameter) preferentially as exosomes and the relatively larger ones (≥130 nm in diameter) as microvesicles. According to this classification, further NTA data showed that increased excretion of both exosome-like small UEVs as well as microvesicle-like large UEVs from patients with T2DM was positively correlated with the progression of the albuminuric stages (Fig. 1*B* and *C*). On single-regression analysis, the number of total, small, and large UEVs was also found to be positively correlated with the ACR (Fig. 1*D*–*F*) and negatively correlated with the estimated glomerular filtration rate (eGFR) in all the subjects (Fig. 1*G*–*I*). However, the number of total UEVs was not correlated with the age, BMI, systolic blood pressure, or HbA_{1c} levels of the subjects (Supplementary Fig. 2*A*–*D*), indicating their marginal impact on the excretion of UEVs in the subjects.

Increased C-Megalin Excretion via UEVs in T2DM Patients

UEVs are known to contain the endocytic receptors megalin and cubilin, in addition to other transporter or channel proteins (12,16,25). C-megalin immunoblotting against urinary first and second pellets confirmed UEV-mediated C-megalin excretion (Fig. 2*A*). Since creatinine-normalized total UEV protein concentration was correlated significantly with creatinine-normalized total UEV number (Spearman rank correlation coefficient = 0.678, $P < 0.001$), we carried out standard immunoblotting using the same amount of UEV proteins to evaluate megalin or other tubular segment marker (16,25) protein content per total UEV protein in different sample types (Fig. 2*B*). We found that megalin protein content per total UEV protein appeared to increase along with the progression of the albuminuric stages in DN, but the other tubular segment markers did not (Fig. 2*B*). The protein content of CD9, an EV marker (25), (as well as CD81 and TSG101, more specific exosome markers) per total UEV protein was not also changed along with the development and progression of DN (Fig. 2*B* and Supplementary Fig. 3*A*–*C*). Thus, using CD9 as an EV internal control, the densitometry ratio between megalin protein content and CD9 protein content in UEVs (i.e., relative megalin protein content per UEV) was evaluated, showing that the ratio increased along with the progression of the disease (Fig. 2*C*). On the other hand, the densitometry ratio between other tubular segment marker proteins and CD9 protein content did not change along with the progression of DN (Supplementary Fig. 3*D*–*H*). The densitometry ratio between megalin protein content and CD9 protein content was also correlated with the ACR (Fig. 2*D*) and eGFR (Fig. 2*E*) but not with the age, BMI, systolic blood pressure, or HbA_{1c} levels of the subjects (Supplementary Fig. 2*E*–*H*). These data indicate that a gradual increase in UEV-mediated C-megalin excretion is characteristically associated with the progression of DN.

When we calculated total C-megalin excretion via UEVs by multiplying the relative C-megalin content per UEV with the corresponding numbers of UEVs, we found that it increased gradually along with the development and progression of DN from the normoalbuminuric stage (Fig. 2*F*), which is consistent with our previous data of direct urinary C-megalin ELISA measurement in T2DM patients (12), and was positively correlated with the ACR (Fig. 2*G*) and negatively correlated with the eGFR (Fig. 2*H*) in single-regression analysis.

As megalin is an endocytic receptor, it is expected to be excreted more via exosomes rather than other types of EVs. We purified exosomes from the total population of UEVs using paramagnetic beads coated with antibodies against CD63, a classic exosomal marker (18), and CD81, a more specific exosomal marker (26), and visualized the beads by TEM to evaluate purification efficiency followed by immunoblotting. TEM showed that the captured UEVs were small and within the size range of exosomes (<130 nm) (Fig. 3*A*). Immunoblot analysis of the lysates of corresponding beads further confirmed the presence of C-megalin within the captured exosomes, indicating exosome-mediated C-megalin excretion (Fig. 3*B* and *C*). We prepared UEVs from the same volume of creatinine-normalized urine samples, applied them to an excess of beads coated with antibodies against CD81, and analyzed purified urinary exosomes by immunoblotting. Megalin content in the purified exosomes was confirmed to increase gradually along with the progression of DN (Fig. 3*D* and *E*).

Immunoelectron microscopy against C-megalin and the podocyte marker podocalyxin (Fig. 3*F*), followed by size distribution analysis of C-megalin–positive and

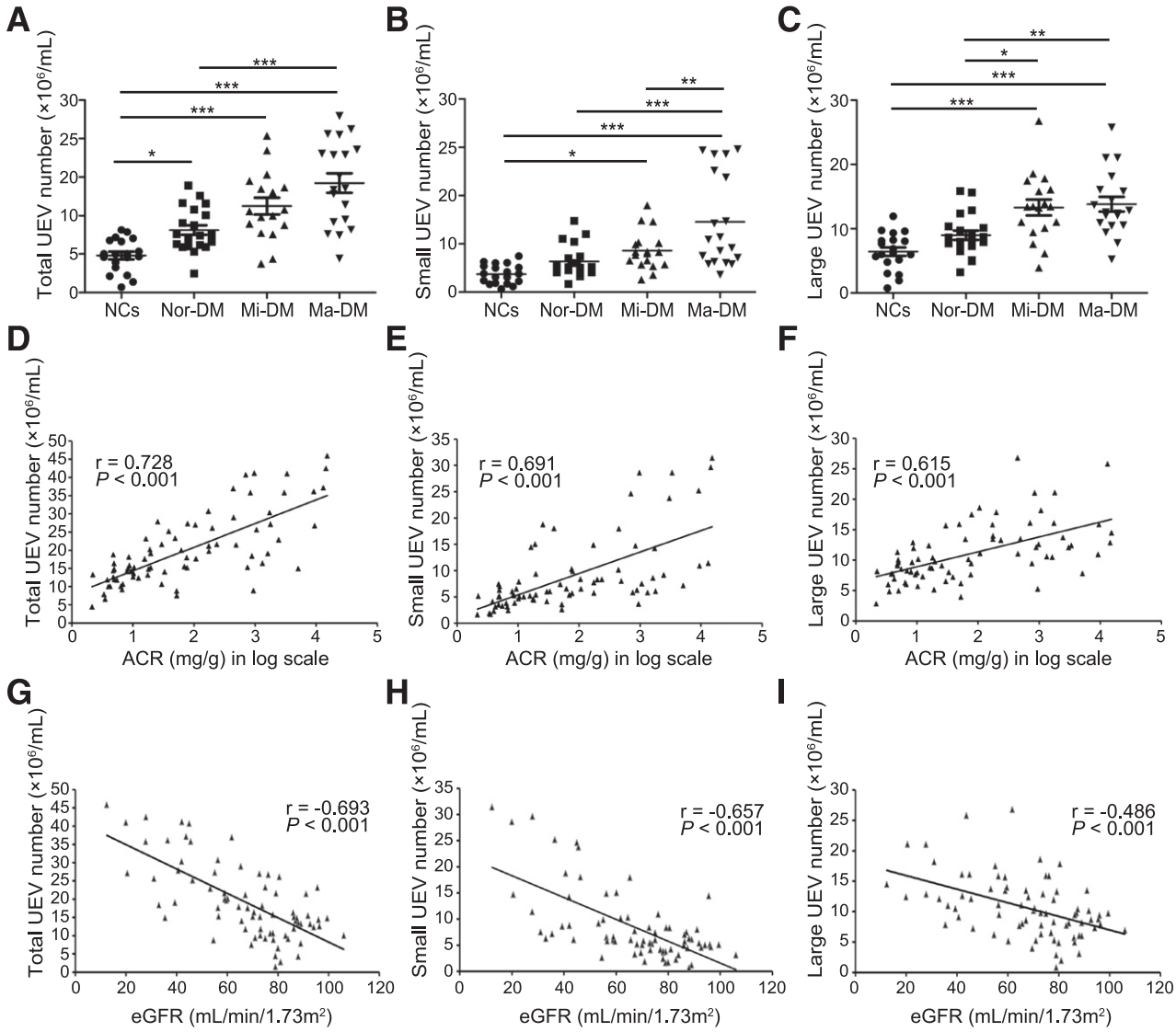

Figure 1—Patients with T2DM excrete more UEVs than NCs. *A*: NTA revealed that, compared with NCs, the total number of excreted UEVs increased in creatinine-standardized urine samples from T2DM patients. The excretion of small UEVs (<130 nm, exosome-like) (*B*) as well as large UEVs (≥130 nm, microvesicle-like) (*C*) increased in T2DM patients compared with NCs. Values are means ± SEM, n = 19, 20, 17, and 19, respectively, for NCs, Nor-DM, Mi-DM, and Ma-DM. *$P < 0.05$, **$P < 0.01$, and ***$P < 0.001$. Single-regression analysis showed that the numbers of total UEVs (*D*) as well as small UEVs (*E*) and large UEVs (*F*) were correlated positively with the ACR, whereas the numbers of total UEVs (*G*) as well as small UEVs (*H*) and large UEVs (*I*) were correlated negatively with the eGFR. r = Spearman rank-correlation coefficient (n = 75).

podocalyxin-positive UEVs from NCs and patients with T2DM, indicated that excretion of urinary C-megalin and podocalyxin was mediated preferentially via exosomes and microvesicles, respectively (Fig. 3*G* and *H*).

Characterization of C-Megalin–Containing UEVs

Next, we purified C-megalin–containing UEVs (mostly exosomes) from the total population of UEVs using GST-RAP–coated glutathione beads in the presence of Ca^{2+}, because RAP is a high-affinity Ca^{2+}-dependent ligand of the extracellular domain of megalin (27). The specificity of GST-RAP binding to megalin in the population of UEVs was confirmed by ligand-blotting analysis (Supplementary Fig. 4*A*). By TEM of the glutathione beads (Supplementary Fig. 4*B*) and subsequent immunoblot analysis of the lysates of the corresponding beads (Supplementary Fig. 4*C*), we showed that the beads effectively and specifically purified C-megalin–containing UEVs.

Exosomes contain large amounts of functional small RNAs including miRNAs for cell-cell communication (28). Therefore, we assessed levels of miRNA-192, which is one of the best characterized miRNAs expressed preferentially and highly in the kidney, in GST-RAP–purified C-megalin–containing UEVs from NCs and patients with T2DM. In comparison with NCs, RNU6-standardized miRNA-192 levels were lower in the early phase of DN and tended

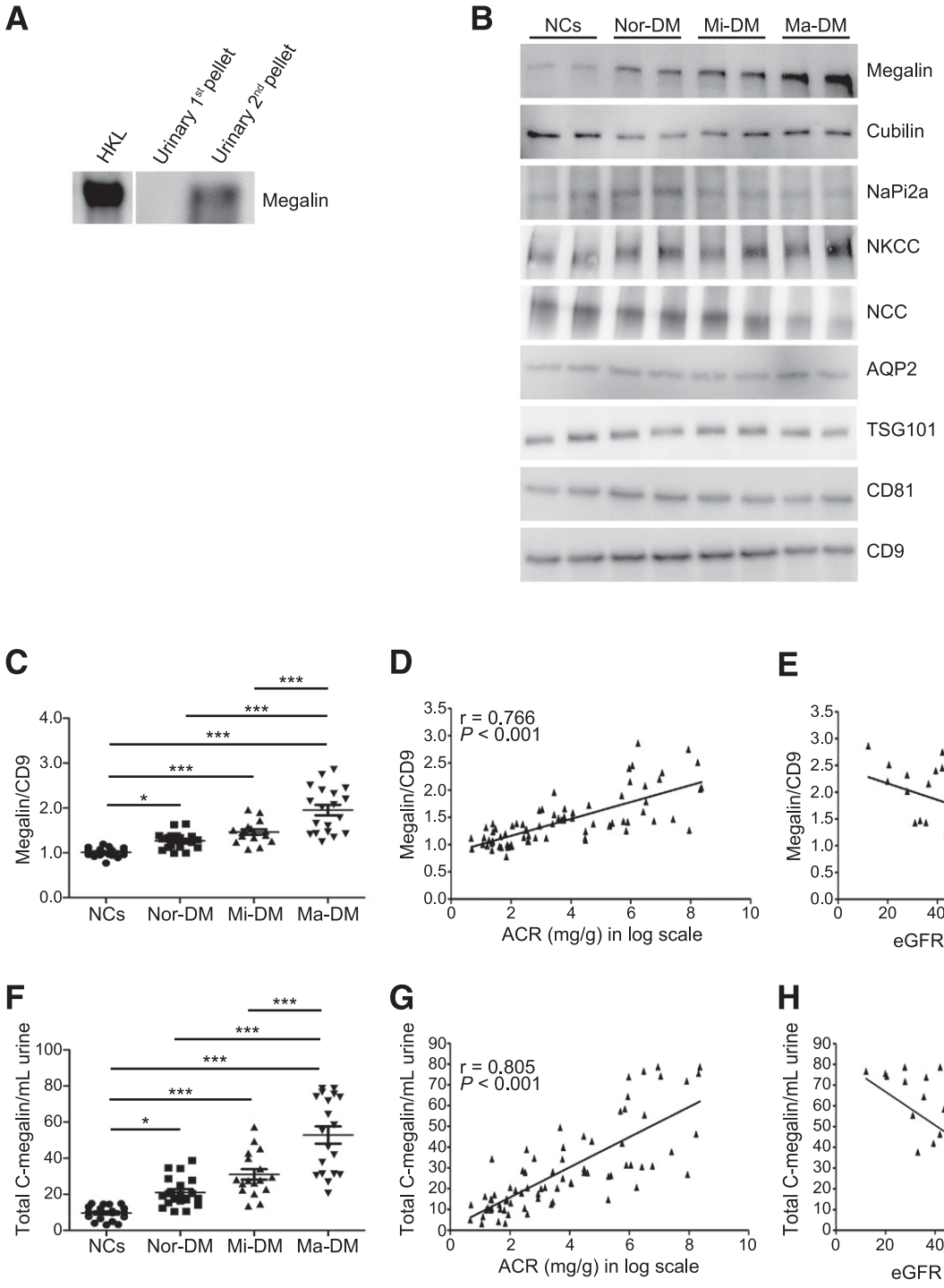

Figure 2—C-megalin excretion via UEVs is increased along with the development and progression of DN in T2DM patients. *A*: C-megalin was detected in the UEV-enriched urinary second pellet (5 μg protein) but not in the urinary first pellet (5 μg) by immunoblotting with an antibody against the COOH-terminal domain of megalin. HKL, human kidney lysates (2 μg). Immunoblots using UEV proteins (10 μg each) from NCs and patients with T2DM against C-megalin and the EV marker protein CD9 (*B*) were followed by densitometry analysis (*C*), which revealed the increased excretion of C-megalin per UEV in patients with T2DM with the progression of DN, whereas the relative excretion of other tubular segment marker proteins such as cubilin (PTEC), Na^+-Pi cotransporter 2a (NaPi2a) (PTEC), Na^+-K^+-$2Cl^-$ cotransporter (NKCC) (thick ascending limb of the loop of Henle), Na^+-Cl^- cotransporter (NCC) (distal tubule), and aquaporin 2 (AQP2) (collecting duct) via UEVs was not correlated with the progression of DN. By single-regression analysis, C-megalin content per UEV (arbitrary units for densitometry analysis of immunoblotting for the ratio between C-megalin and CD9) was found to be positively correlated with ACR (*D*) and negatively correlated with eGFR (*E*). Urinary total C-megalin excretion per milliliter creatinine-standardized urine via UEVs was calculated by multiplying CD9-standardized C-megalin values with the corresponding UEV number for each subject. *F*: Total C-megalin excretion via UEVs (arbitrary units) increased gradually along with the development and progression of DN. Single-regression analysis showed that total C-megalin excretion via UEVs (arbitrary units) was correlated positively with ACR (*G*) and eGFR (*H*). Values are means ± SEM, n = 19, 20, 17, and 19, respectively, for NCs, Nor-DM, Mi-DM, and Ma-DM. $^*P < 0.05$ and $^{***}P < 0.001$. n = 75.

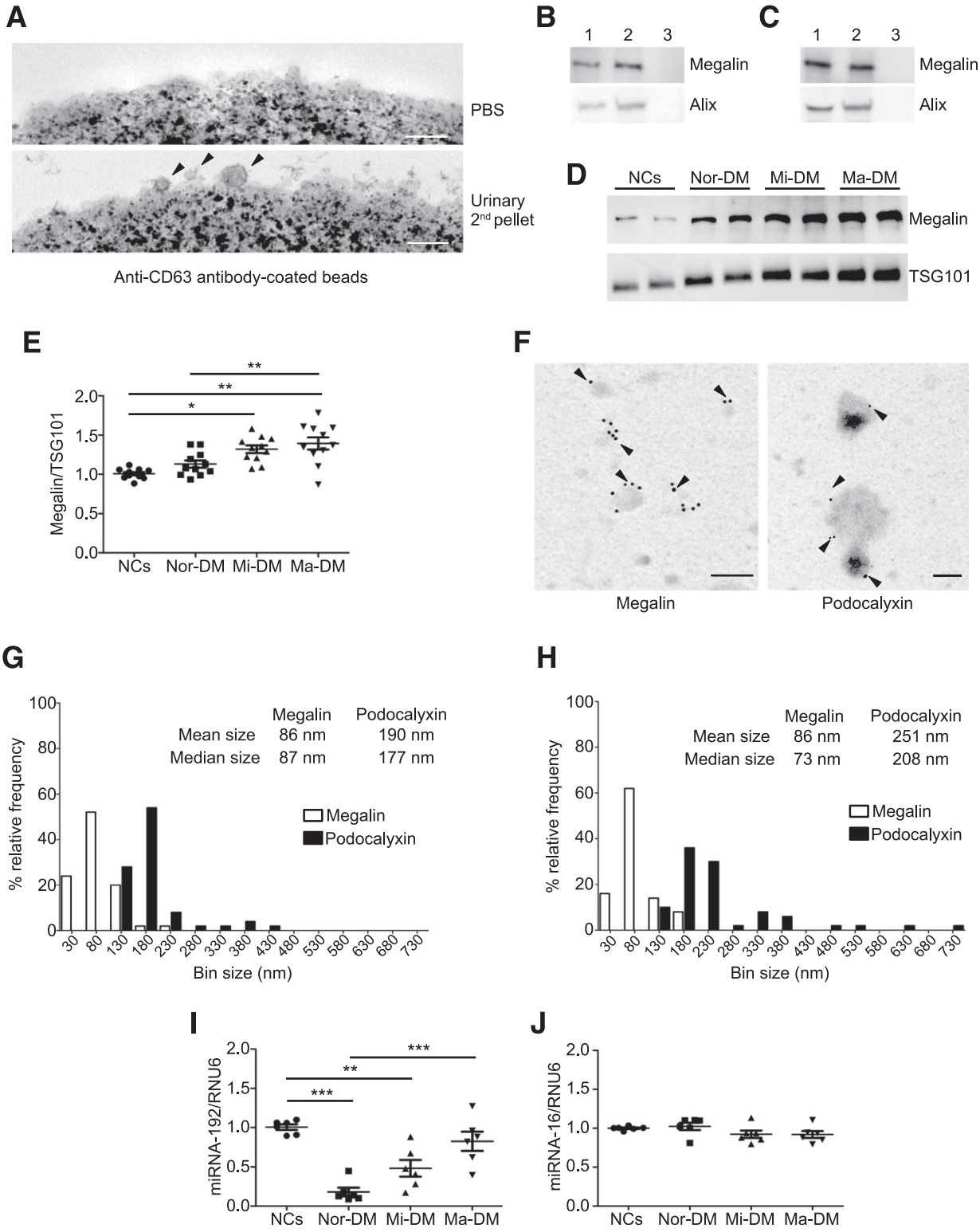

Figure 3—C-megalin is excreted mainly via exosomes with different miRNA-192 content along with the development and progression of DN. *A*: Exosomes were purified from the total population of UEVs using anti-CD63 antibody–coated paramagnetic beads followed by TEM. Small UEVs on the surface of the beads (arrowheads), when treated with urinary second pellets, confirmed the efficacy of exosomal purification. Scale bars = 100 nm. *B*: Immunoblot analysis of the lysates of the corresponding beads for C-megalin and the exosome marker protein Alix, confirming that C-megalin is contained in exosomes. *C*: For data confirmation, as described above, exosomes were purified from the total population of UEVs using anti-CD81 antibody–coated paramagnetic beads followed by immunoblotting. 1, urinary second pellet protein (5 μg); 2, lysate supernatant of anti-CD63 (*B*) or anti-CD81 (*C*) antibody–coated beads incubated with urinary second pellet; and 3, lysate supernatant of anti-CD63 (*B*) or anti-CD81 (*C*) antibody–coated beads incubated with PBS. *A*–*C*: The urinary exosomes were representatively prepared from an Mi-DM patient. Immunoblot against C-megalin and the exosomal marker TSG101 using exosomal preparations from creatinine-normalized urine samples (*D*) and their densitometric analysis (*E*) revealed that total exosomal C-megalin

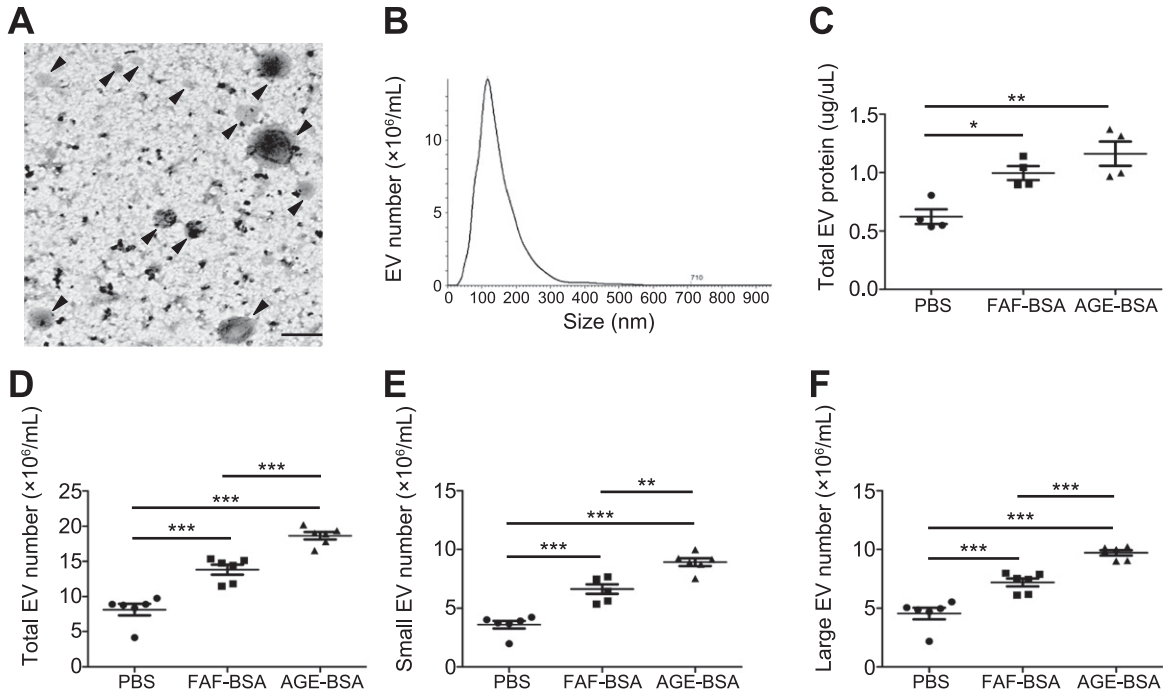

Figure 4—Excretion of EVs from IRPTCs is increased under the influence of protein overload and treatment with AGE-modified proteins. *A*: A simple observation of EVs from IRPTCs by TEM showed vesicles of different sizes, as indicated by the arrowheads. Scale bar = 200 nm. *B*: Size distribution and mode size analysis of EVs by NTA indicated that IRPTC-derived EVs showed a similar size distribution pattern and mode size (117 nm) as UEVs. *C*: Total EV protein concentration increased gradually when the cells were treated with FAF-BSA or AGE-BSA compared with PBS (vehicle), indicating a probable increase in EV excretion from IRPTCs. *D*: Size distribution study by NTA also showed a gradual increase in the total number of EVs excreted from IRPTCs when treated with FAF-BSA or AGE-BSA. Similar to UEVs, the excretion of smaller EVs (<130 nm, exosome-like) (*E*) and larger EVs (≥130 nm, microvesicle-like) (*F*) increased in the groups treated with FAF-BSA or AGE-BSA. Values are means ± SEM, $n = 6$ for each group. $^{*}P < 0.05$, $^{**}P < 0.01$, and $^{***}P < 0.001$.

to increase with the progression of DN (Fig. 3*I*). However, miRNA-16, an endogenous control miRNA, did not change with disease progression (Fig. 3*J*), indicating that there are DN stage-related differences in miRNA content in C-megalin–containing UEVs with putative pathophysiological relevance.

Protein Overload and AGE-Modified Protein Treatment Increase Exosome-Mediated C-Megalin Excretion From Cultured IRPTCs

To establish the molecular mechanism underlying the increased excretion of UEVs in patients with T2DM, we treated IRPTCs with FAF-BSA as a protein overload model and AGE-BSA as a glycated protein load model. Both FAF-BSA and AGE-BSA are the endocytic ligands of megalin (7,8). Thereafter, we collected IRPTC-derived EVs from the conditioned media. As with UEVs, TEM and NanoSight were used to characterize the IRPTC-derived EVs. TEM revealed that the majority of EVs had a typical size of 50–130 nm, which identified them as exosomes isolated from different cell lines (Fig. 4*A* and *B*) (15,29). By NTA, those EVs were confirmed to be exosome enriched as evidenced by their mode size of 117 nm (Fig. 4*B*). Total EV protein concentration data indicated that EV excretion was increased by treatment of the cells with FAF-BSA and were further elevated with AGE-BSA, compared with vehicle (PBS) treatment (Fig. 4*C*). These findings were further confirmed by NTA (Fig. 4*D*). It also confirmed that the number of exosome-like small EVs (<130 nm) and microvesicle-like large EVs (≥130 nm) was increased by FAF-BSA treatment and further elevated by AGE-BSA treatment (Fig. 4*E* and *F*).

content and its content per exosome increased gradually along with the progression of DN. Values are means ± SEM, $n = 11$ for each group. $^{*}P < 0.05$ and $^{**}P < 0.01$. *F*: Immunoelectron microscopy revealed that the relatively smaller vesicles (putative exosomes) were immunopositive for C-megalin (indicated by arrowheads), whereas the larger vesicles (putative microvesicles) were positive for podocalyxin (also indicated by arrowheads), representatively shown in UEVs prepared from an Mi-DM patient. Scale bars = 100 nm. The mean and median sizes of the C-megalin–positive UEVs from NCs and patients with T2DM were found to be in the range of exosomes (<130 nm), whereas podocalyxin-positive UEVs were in the size range of microvesicles (≥130 nm) in 20 randomly selected C-megalin– and podocalyxin-positive UEVs, respectively, from each individual NC (*G*) and T2DM (*H*) patient ($n = 5$, each). *I*: Compared with C-megalin–containing UEVs purified using GST-RAP from NCs, miRNA-192 content in those from T2DM patients changed along with the development and progression of DN, as measured by quantitative RT-PCR. Values are means ± SEM, $n = 6$ for each group. $^{**}P < 0.01$ and $^{***}P < 0.001$. *J*: There was no such change in the content of miRNA-16, an endogenous control miRNA.

C-megalin immunoblotting followed by densitometry analysis revealed a similar increase in C-megalin excretion per the content of exosomal marker Alix when the cells were treated with FAF-BSA and AGE-BSA (Fig. 5*A* and *B*), whereas the cellular expression of megalin was not changed by either treatment (Fig. 5*C* and *D*). To prove exosome-mediated C-megalin excretion by such treatments, an established exosome excretion inhibitor, GW4869 (30), which acts on neutral sphingomyelinase to inhibit exosome production, was added to IRPTCs, leading to decreased EV protein concentration in the culture media, even when the cells were treated with AGE-BSA (Fig. 5*E*). As a result of exosome inhibition, EV-mediated excretion of C-megalin, standardized by Alix, was also inhibited, indicating that increased C-megalin excretion by AGE-BSA treatment is mediated via exosomes (Fig. 5*F* and *G*), whereas the cellular expression of total megalin was not changed (Fig. 5*H* and *I*). Exosome inhibitor treatment along with FAF-BSA also

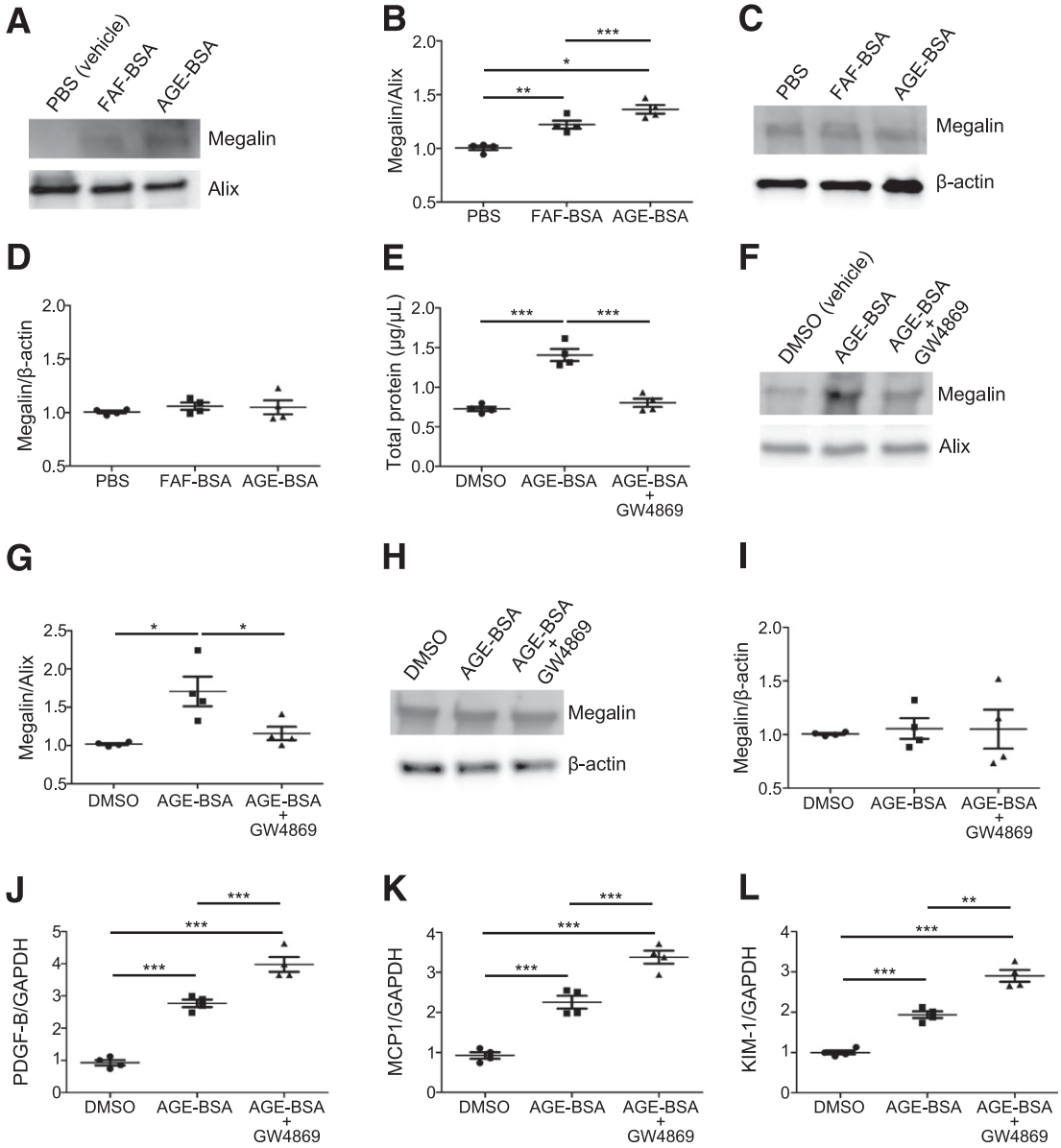

Figure 5—Protein overload and AGE-modified protein treatment both lead to increased C-megalin excretion via exosomes from IRPTCs. Immunoblots with the same amount of EV proteins (7.5 μg) from culture media against C-megalin and the exosomal marker protein Alix followed by densitometry analysis revealed that C-megalin excretion via EVs was enhanced from IRPTCs when they were treated with FAF-BSA and maximized with AGE-BSA (*A* and *B*), whereas megalin expression at the cellular level was the same in all groups (*C* and *D*). By incubating IRPTCs with the exosome inhibitor GW4869 (4 μmol/L) for 48 h, total EV protein concentration (*E*) and excretion of C-megalin via EVs (*F* and *G*) decreased, indicating that C-megalin excretion from IRPTCs is exocytosis mediated. *H* and *I*: The cellular expression of megalin was not changed by exosome inhibition. Increased mRNA expression of pathological markers such as platelet-derived growth factor subunit B (PDGF-B) (*J*), monocyte chemoattractant protein-1 (MCP-1) (*K*), and kidney injury molecule-1 (KIM-1) (*L*) was detected by exosome inhibition in the presence of AGE-BSA. Values are means ± SEM, $n = 4$ for each group. *$P < 0.05$, **$P < 0.01$, and ***$P < 0.001$.

showed similar results (data not shown). Increased mRNA expression of platelet-derived growth factor subunit B and monocyte chemoattractant protein 1, which are profibrotic factors, as well as kidney injury molecule 1, a PTEC injury marker protein, in IRPTCs treated with AGE-BSA was detected by exosome inhibition (Fig. 5*J–L*), indicating that increased exosome release by PTECs might be a protective mechanism of the cells.

AGE-BSA Induces Lysosomal Dysfunction and Causes Increased MVB Formation and Exosomal C-Megalin Excretion From IRPTCs

It is generally accepted that, in PTECs, filtrated albumin undergoes megalin/cubilin-mediated endocytosis and is transferred to lysosomes for further degradation (8). We performed LysoTracker Deep Red staining for lysosomal morphology, which showed an accumulation of giant lysosomes (>1 μm) around the nucleus of IRPTCs treated with AGE-BSA, but not FAF-BSA, for 24 h (Fig. 6*A*). On quantification of the giant lysosomes standardized by cellular area, we found a significant increase in their number in AGE-BSA–treated IRPTCs, indicating lysosomal dysfunction (Fig. 6*B*). In correlation with the increased accumulation of giant lysosomes, the augmented expression of lysosomal-associated membrane protein 1 was also found in AGE-BSA–treated cells, indicating an increased number and size of lysosomes, a hallmark of lysosomal dysfunction (Fig. 6*C* and *D*) (31,32). Furthermore, AGE-BSA treatment for 48 h caused increased MVB formation, as indicated by the augmented cellular expression of the endosomal sorting complex required for transport–associated proteins TSG101 (Fig. 6*E* and *F*) and Alix (Fig. 6*G* and *H*) (33). Indeed, megalin-containing vesicles were found to be recruited into MVBs in those cells treated particularly with AGE-BSA (and also with FAF-BSA) for 48 h (Supplementary Fig. 5). Thus, we speculated that AGE-BSA treatment leads to apparent lysosomal dysfunction in IRPTCs within 24 h, which thereafter results in increased MVB formation and excretion of exosomes containing C-megalin.

To verify the lysosomal dysfunction–mediated increase of exosomal C-megalin excretion, we treated IRPTCs with two potent lysosomal inhibitors with different modes of

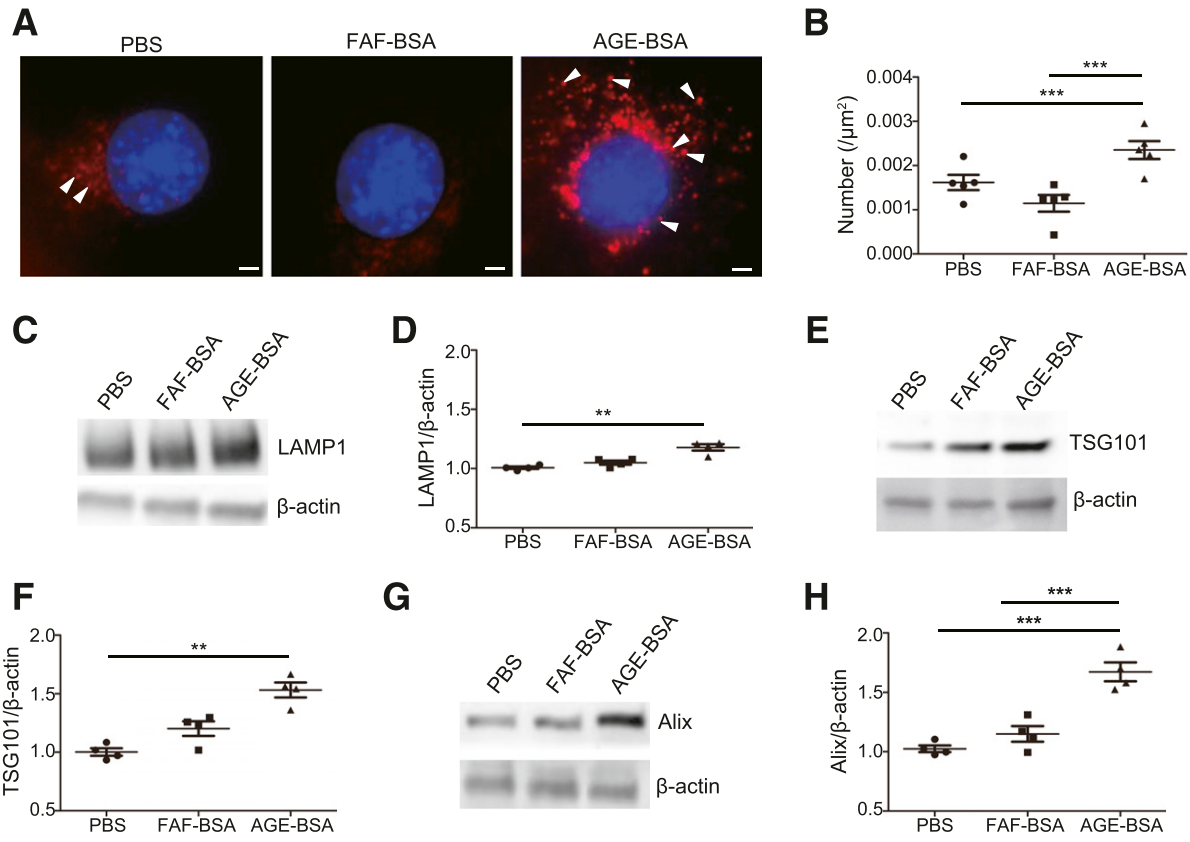

Figure 6—AGE-modified protein treatment leads to lysosomal dysfunction and increased MVB formation in IRPTCs. *A* and *B*: By lysosome (red) and nucleus (blue) staining, giant lysosomes (>1 μm) (arrowheads) were found to be significantly increased in number, standardized by the area of the cells, particularly in the cytoplasm of AGE-BSA–treated IRPTCs, compared with the other groups. Scale bars = 5 μm. *C* and *D*: By immunoblotting, it was found that AGE-BSA treatment of IRPTCs for 24 h increased the expression of one of the most abundant lysosomal components, lysosomal-associated membrane protein 1 (LAMP1), indicating lysosomal dysfunction. AGE-BSA treatment of the cells for 48 h increased the expression of the endosomal sorting complex required for transport protein TSG101 (*E* and *F*) and its interacting protein Alix (*G* and *H*), indicating increased MVB formation, a prerequisite for enhanced exosome release. Values are means ± SEM, $n = 4$ for each group. $^{**}P < 0.01$ and $^{***}P < 0.001$.

actions, namely bafilomycin A1, an inhibitor of vacuolar-type H^+-ATPase (34), and chloroquine phosphate, a lysosomotropic agent that increases lysosomal pH (35), and collected excreted EVs from the culture media. We found an increase in the cellular expression of TSG101 (Fig. 7*A* and *B*) and Alix (Fig. 7*C* and *D*) and increased C-megalin excretion per exosome (Fig. 7*E* and *F*) but not overall cellular C-megalin expression (Fig. 7*G* and *H*), indicating that lysosomal dysfunction caused an increase in MVB formation and exosomal C-megalin excretion.

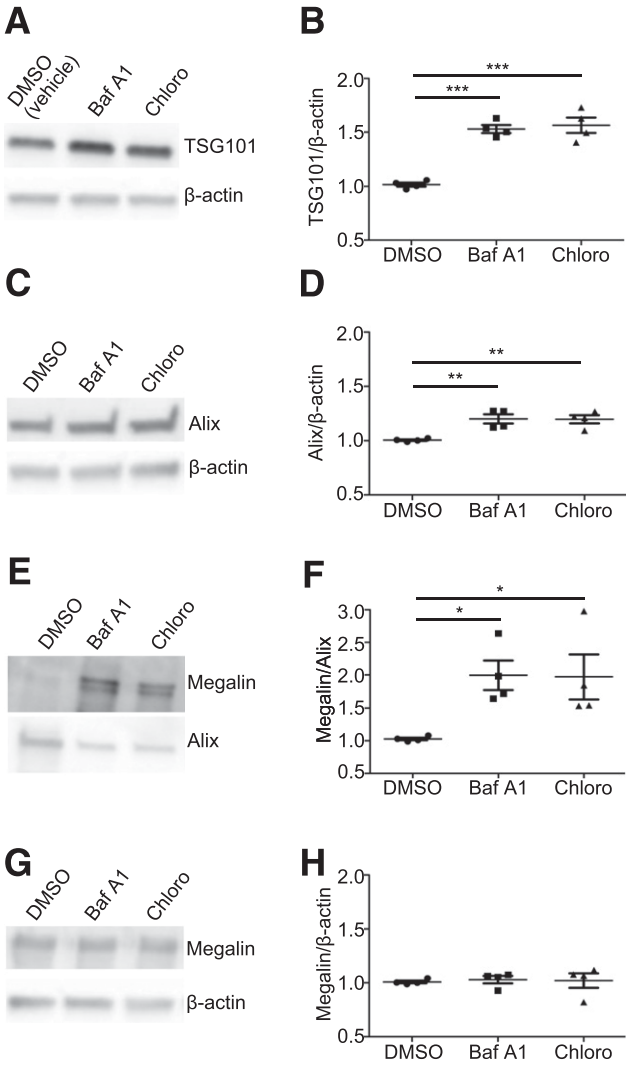

Figure 7—Chemically induced lysosomal dysfunction enhances MVB production and increases exosomal C-megalin excretion. Treatment of IRPTCs with the lysosome inhibitors bafilomycin A1 (Baf A1, 50 nmol/L) or chloroquine phosphate (Chloro, 50 μmol/L) for 48 h enhanced MVB formation, as evidenced by the increased cellular expression of TSG101 (*A* and *B*) and Alix (*C* and *D*). Exosome-mediated C-megalin excretion was also increased in lysosome-dysfunctional cells (*E* and *F*), whereas the cellular expression of megalin was not altered by the lysosome inhibitors (*G* and *H*). Values are means ± SEM, $n = 4$ for each group. *$P < 0.05$, **$P < 0.01$, and ***$P < 0.001$.

Urinary C-Megalin Excretion via UEVs Is Increased in Mice Fed an HFD

Megalin mediates autolysosomal dysfunction in PTECs, which leads to tubuloglomerular alterations in mice fed an HFD (9). In this obesity-related diabetes model, we found an increased number of total, small, and large UEVs compared with mice fed an NFD (Fig. 8*A–C*). Also, urinary C-megalin excretion increased via UEVs in HFD-fed mice compared with NFD-fed mice (Fig. 8*D* and *E*).

DISCUSSION

Previously, we established a urinary C-megalin ELISA that was potentially useful for the early diagnosis and evaluation of the severity of DN in patients with T2DM (12). Here, we established that elevated urinary C-megalin excretion in patients with T2DM is associated with an increased number of urinary exosomes as well as C-megalin content per exosome. Besides, patients with T2DM may also excrete an increased number of urinary microvesicles, probably partly from podocytes (17,19).

Low–molecular-weight protein markers for PTEC injury, such as α_1-microglobulin, β_2-microglobulin, and liver-type fatty acid–binding protein, are filtered by glomeruli and reabsorbed by PTECs via megalin (8). Not only physiologically important substrates, including insulin, albumin, and vitamin D–binding protein, but also some substances, such as AGEs, myeloma light chain, and fatty acid–rich proteins, have been identified as toxic ligands of megalin, leading to PTEC injury (9,36).

Serum AGE levels reflect the severity of DN (37) and are reportedly involved in the pathogenesis of DN (38). High-concentration protein overload in cultured PTECs was found to lead to lysosomal dysfunction (39,40); however, the protein concentrations used (8 and 20 mg/mL, respectively) in these experiments were much higher than in ours (1 mg/mL). Although protein overload with FAF-BSA did not result in significant lysosomal dysfunction compared with vehicle-treated cells in the current study, overload with AGE-modified BSA caused apparent lysosomal dysfunction, again confirming AGE-mediated cytotoxicity in PTECs via megalin (41,42). Hence, the increased excretion of EVs by FAF-BSA–treated IRPTCs in this study may be associated with increased endocytosis.

Recently, we reported that megalin-mediated autolysosomal dysfunction in PTECs is primarily important for the development of kidney disease in an HFD-induced diabetes model (9). In the current study, we found that exocytosis-mediated urinary C-megalin excretion increased along with the development and progression of DN and that lysosomal dysfunction in AGE-BSA–treated IRPTCs leads to an increase in MVB formation and exocytosis-mediated C-megalin excretion. Indeed, we found that urinary C-megalin excretion increased via UEVs in HFD-fed mice compared with NFD-fed mice. As exosomes are formed within the endosomal network and late endosomes (MVBs) are targeted to fuse either with lysosomes for further degradation or with the plasma membrane

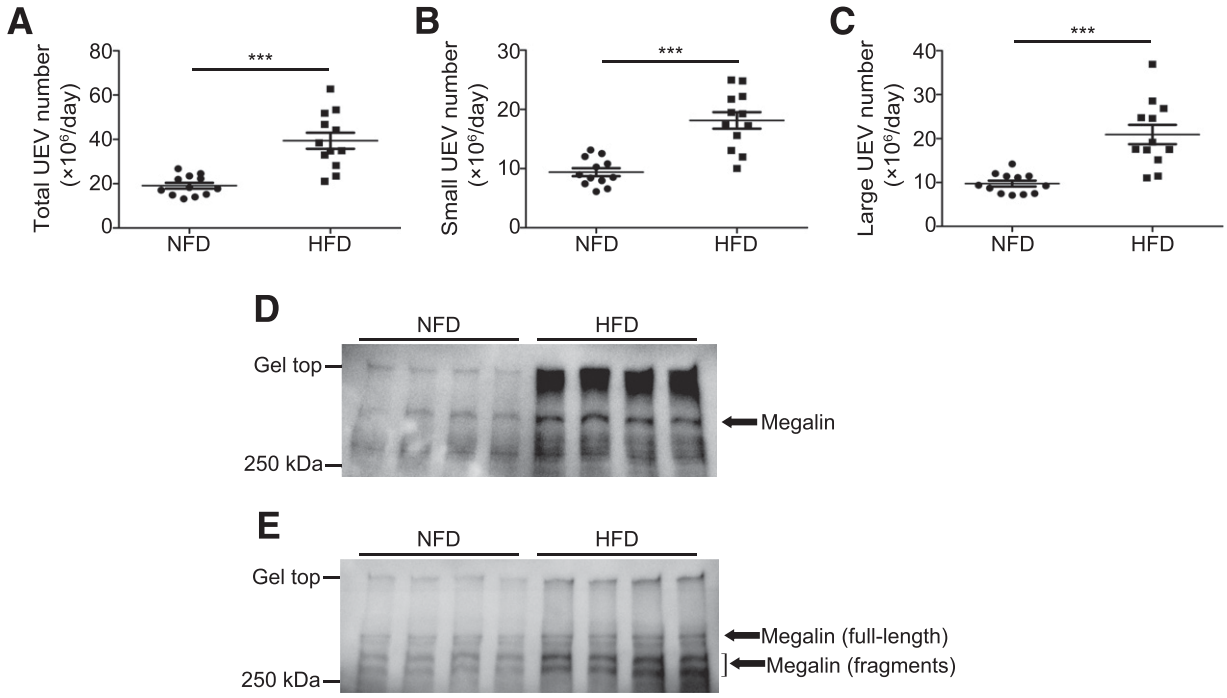

Figure 8—Urinary C-megalin excretion via UEVs is increased in mice fed an HFD. NTA revealed that the number of total (*A*), small (<130 nm) (*B*), and large (≥130 nm) (*C*) UEVs increased in volume-standardized urine samples collected for 72 h from C57BL/6J mice fed an HFD from 11 weeks of age for 4 weeks compared with mice fed an NFD. Values are means ± SEM, $n = 12$ for each group. ***$P < 0.001$. *D*: Immunoblots of volume-standardized urine samples collected for 24 h from mice fed an HFD or NFD for 6 weeks against C-megalin revealed an apparently increased urinary excretion of C-megalin in HFD-fed mice compared with NFD-fed mice. *E*: Immunoblots of UEVs prepared from volume-standardized urine samples collected for 48 h from mice fed an HFD or NFD for 6 weeks against C-megalin also revealed an increased UEV-mediated megalin excretion in HFD-fed mice, although megalin in the preparation of UEVs appeared to be degraded into fragments.

for excreting exosomes, lysosomal dysfunction should result in increased MVB production, megalin recruitment in MVBs, and finally the release of exosomes containing megalin. Thus, urinary C-megalin excretion via exocytosis is linked with the megalin-mediated pathogenesis underlying the development and progression of DN.

Exosomal miRNAs and exosome-mediated miRNA transfer are increasingly recognized as critical players in gene regulation and various diseases including DN (28,43). After treatment with transforming growth factor-β, miRNA-192 expression is increased in cultured mesangial cells (44) but is decreased in PTECs (22). miRNA-192 was also found to be increased in human kidney in both hypertensive nephrosclerosis (45) and IgA nephropathy (46). Compared with NCs, PTEC-derived C-megalin–containing exosomes in normoalbuminuric T2DM patients contained less miRNA-192, which might be a protective mechanism against miRNA-192 loss in PTECs. In contrast, miRNA-192 might be produced more in PTECs with the progression of DN, resulting in increased miRNA-192 excretion via exosomes in the advanced stages of DN. Exosome inhibition in cultured IRPTCs also increased pathological reactions, indicating that exosome excretion may be a beneficial phenomenon for PTECs. It remains to be studied whether C-megalin–containing exosomes have a role in the transfer of miRNA-192 to cells in the downstream tubules or urinary tract.

In conclusion, protein overload or AGE-mediated PTEC injury should increase exocytosis-mediated urinary C-megalin along with the progression of DN. Thus, megalin-mediated quantitative or qualitative protein metabolic load to residual functioning nephrons should be the mechanism underlying the increase in urinary C-megalin excretion in T2DM patients, which could be a novel biomarker associated directly with the pathogenesis of DN.

Acknowledgments. The authors thank Dr. Julie R. Ingelfinger (Massachusetts General Hospital) for the gift of the experimental material described in RESEARCH DESIGN AND METHODS and Dr. Masaaki Komatsu, Dr. Reika Kaneko, Akiko Seino, Nanako Sugita, Koichi Komochi, Masaaki Nameta, and Kazumasa Sato at Niigata University for their technical assistance. The authors also thank ThinkSCIENCE for help in the preparation of the manuscript.

Funding. This work was supported in part by Grants-in-Aid for Scientific Research from the Ministry of Education, Culture, Sports, Science, and Technology of Japan to M.Ho. (grant 26860630) and A.S. (grant 26461216) and by Grants-in-Aid for the Practical Research Project for Renal Diseases from the Japan Agency for Medical Research and Development.

Duality of Interest. S.K. and A.S. received research grants from DENKA SEIKEN Co., Ltd. No other potential conflicts of interest relevant to this article were reported.

Author Contributions. S.D. designed the study, researched data, and wrote the manuscript. S.K. and P.S. researched data, contributed to the discussion, and reviewed the manuscript. M.Ho., T.Is., R.K., H.Ka., T.Ii., S.G., and Y.S. collected clinical data and urine samples, contributed to the discussion, and reviewed the manuscript. Y.Y. and T.O. performed NTA of EVs and reviewed

the manuscript. K.T. and Y.Hig. contributed to the animal experiments. M.Ha., H.Ku., and Y.Hir. contributed to the experiments for podocalyxin. I.N. contributed to the discussion and reviewed the manuscript. A.S. designed the study and wrote the manuscript. S.D. and A.S. are the guarantors of this work and, as such, had full access to all the data in the study and take responsibility for the integrity of the data and the accuracy of the data analysis.

Prior Presentation. Parts of this study were presented in abstract form at Kidney Week 2015—American Society of Nephrology 48th Annual Meeting, San Diego, CA, 3–8 November 2015.

References

1. Pugliese G. Updating the natural history of diabetic nephropathy. Acta Diabetol 2014;51:905–915
2. Mehdi U, Toto RD. Anemia, diabetes, and chronic kidney disease. Diabetes Care 2009;32:1320–1326
3. Vallon V. The proximal tubule in the pathophysiology of the diabetic kidney. Am J Physiol Regul Integr Comp Physiol 2011;300:R1009–R1022
4. Nangaku M. Chronic hypoxia and tubulointerstitial injury: a final common pathway to end-stage renal failure. J Am Soc Nephrol 2006;17:17–25
5. Levey AS, Cattran D, Friedman A, et al. Proteinuria as a surrogate outcome in CKD: report of a scientific workshop sponsored by the National Kidney Foundation and the US Food and Drug Administration. Am J Kidney Dis 2009;54:205–226
6. Saito A, Pietromonaco S, Loo AK, Farquhar MG. Complete cloning and sequencing of rat gp330/"megalin," a distinctive member of the low density lipoprotein receptor gene family. Proc Natl Acad Sci U S A 1994;91:9725–9729
7. Saito A, Sato H, Iino N, Takeda T. Molecular mechanisms of receptor-mediated endocytosis in the renal proximal tubular epithelium. J Biomed Biotechnol 2010;2010:403272
8. De S, Kuwahara S, Saito A. The endocytic receptor megalin and its associated proteins in proximal tubule epithelial cells. Membranes (Basel) 2014;4:333–355
9. Kuwahara S, Hosojima M, Kaneko R, et al. Megalin-mediated tubuloglomerular alterations in high-fat diet-induced kidney disease. J Am Soc Nephrol 2016;27:1996–2008
10. Vlassara H. The AGE-receptor in the pathogenesis of diabetic complications. Diabetes Metab Res Rev 2001;17:436–443
11. Saito A, Takeda T, Sato K, et al. Significance of proximal tubular metabolism of advanced glycation end products in kidney diseases. Ann N Y Acad Sci 2005; 1043:637–643
12. Ogasawara S, Hosojima M, Kaseda R, et al. Significance of urinary full-length and ectodomain forms of megalin in patients with type 2 diabetes. Diabetes Care 2012;35:1112–1118
13. Ji H, Chen M, Greening DW, et al. Deep sequencing of RNA from three different extracellular vesicle (EV) subtypes released from the human LIM1863 colon cancer cell line uncovers distinct miRNA-enrichment signatures. PLoS One 2014;9:e110314
14. Lee Y, El Andaloussi S, Wood MJ. Exosomes and microvesicles: extracellular vesicles for genetic information transfer and gene therapy. Hum Mol Genet 2012;21(Suppl. R1):R125–R134
15. Gray WD, French KM, Ghosh-Choudhary S, et al. Identification of therapeutic covariant microRNA clusters in hypoxia-treated cardiac progenitor cell exosomes using systems biology. Circ Res 2015;116:255–263
16. Gonzales PA, Pisitkun T, Hoffert JD, et al. Large-scale proteomics and phosphoproteomics of urinary exosomes. J Am Soc Nephrol 2009;20:363–379
17. Burger D, Thibodeau JF, Holterman CE, Burns KD, Touyz RM, Kennedy CR. Urinary podocyte microparticles identify prealbuminuric diabetic glomerular injury. J Am Soc Nephrol 2014;25:1401–1407
18. Hiemstra TF, Charles PD, Gracia T, et al. Human urinary exosomes as innate immune effectors. J Am Soc Nephrol 2014;25:2017–2027
19. Hara M, Yamagata K, Tomino Y, et al. Urinary podocalyxin is an early marker for podocyte injury in patients with diabetes: establishment of a highly sensitive ELISA to detect urinary podocalyxin. Diabetologia 2012;55:2913–2919
20. Orlando RA, Farquhar MG. Functional domains of the receptor-associated protein (RAP). Proc Natl Acad Sci U S A 1994;91:3161–3165
21. Hama H, Saito A, Takeda T, et al. Evidence indicating that renal tubular metabolism of leptin is mediated by megalin but not by the leptin receptors. Endocrinology 2004;145:3935–3940
22. Krupa A, Jenkins R, Luo DD, Lewis A, Phillips A, Fraser D. Loss of MicroRNA-192 promotes fibrogenesis in diabetic nephropathy. J Am Soc Nephrol 2010;21:438–447
23. Westwood ME, McLellan AC, Thornalley PJ. Receptor-mediated endocytic uptake of methylglyoxal-modified serum albumin. Competition with advanced glycation end product-modified serum albumin at the advanced glycation end product receptor. J Biol Chem 1994;269:32293–32298
24. Livshits MA, Khomyakova E, Evtushenko EG, et al. Isolation of exosomes by differential centrifugation: theoretical analysis of a commonly used protocol. Sci Rep 2015;5:17319
25. Kowal J, Arras G, Colombo M, et al. Proteomic comparison defines novel markers to characterize heterogeneous populations of extracellular vesicle subtypes. Proc Natl Acad Sci U S A 2016;113:E968–E977
26. Pisitkun T, Shen RF, Knepper MA. Identification and proteomic profiling of exosomes in human urine. Proc Natl Acad Sci U S A 2004;101:13368–13373
27. Orlando RA, Kerjaschki D, Kurihara H, Biemesderfer D, Farquhar MG. gp330 associates with a 44-kDa protein in the rat kidney to form the Heymann nephritis antigenic complex. Proc Natl Acad Sci U S A 1992;89:6698–6702
28. Valadi H, Ekström K, Bossios A, Sjöstrand M, Lee JJ, Lötvall JO. Exosome-mediated transfer of mRNAs and microRNAs is a novel mechanism of genetic exchange between cells. Nat Cell Biol 2007;9:654–659
29. Kadiu I, Narayanasamy P, Dash PK, Zhang W, Gendelman HE. Biochemical and biologic characterization of exosomes and microvesicles as facilitators of HIV-1 infection in macrophages. J Immunol 2012;189:744–754
30. Trajkovic K, Hsu C, Chiantia S, et al. Ceramide triggers budding of exosome vesicles into multivesicular endosomes. Science 2008;319:1244–1247
31. Jerome WG, Netherland-Van Dyke CD, Romer CE. Autophagy exacerbates the lysosomal dysfunction of late-stage atherosclerosis. Microsc Microanal 2013; 19:214–215
32. Usenovic M, Tresse E, Mazzulli JR, Taylor JP, Krainc D. Deficiency of ATP13A2 leads to lysosomal dysfunction, α-synuclein accumulation, and neurotoxicity. J Neurosci 2012;32:4240–4246
33. Montoya M. An ESCRT for daughters. Nat Struct Mol Biol 2007;14:579
34. Yoshimori T, Yamamoto A, Moriyama Y, Futai M, Tashiro Y. Bafilomycin A1, a specific inhibitor of vacuolar-type H(+)-ATPase, inhibits acidification and protein degradation in lysosomes of cultured cells. J Biol Chem 1991; 266:17707–17712
35. Dunmore BJ, Drake KM, Upton PD, Toshner MR, Aldred MA, Morrell NW. The lysosomal inhibitor, chloroquine, increases cell surface BMPR-II levels and restores BMP9 signalling in endothelial cells harbouring BMPR-II mutations. Hum Mol Genet 2013;22:3667–3679
36. Nielsen R, Christensen EI, Birn H. Megalin and cubilin in proximal tubule protein reabsorption: from experimental models to human disease. Kidney Int 2016;89:58–67
37. Berg TJ, Bangstad HJ, Torjesen PA, Osterby R, Bucala R, Hanssen KF. Advanced glycation end products in serum predict changes in the kidney morphology of patients with diabetes mellitus. Metabolism 1997;46:661–665
38. Vlassara H. Protein glycation in the kidney: role in diabetes and aging. Kidney Int 1996;49:1795–1804
39. Liu WJ, Xu BH, Ye L, et al. Urinary proteins induce lysosomal membrane permeabilization and lysosomal dysfunction in renal tubular epithelial cells. Am J Physiol Renal Physiol 2015;308:F639–F649
40. Liu D, Wen Y, Tang TT, et al. Megalin/cubulin-lysosome-mediated albumin reabsorption is involved in the tubular cell activation of NLRP3 inflammasome and tubulointerstitial inflammation. J Biol Chem 2015;290:18018–18028

41. Liu WJ, Shen TT, Chen RH, et al. Autophagy-lysosome pathway in renal tubular epithelial cells is disrupted by advanced glycation end products in diabetic nephropathy. J Biol Chem 2015;290:20499–20510
42. Song YM, Song SO, You YH, et al. Glycated albumin causes pancreatic β-cells dysfunction through autophagy dysfunction. Endocrinology 2013;154:2626–2639
43. Kato M, Arce L, Natarajan R. MicroRNAs and their role in progressive kidney diseases. Clin J Am Soc Nephrol 2009;4:1255–1266
44. Kato M, Zhang J, Wang M, et al. MicroRNA-192 in diabetic kidney glomeruli and its function in TGF-β-induced collagen expression via inhibition of E-box repressors. Proc Natl Acad Sci U S A 2007;104:3432–3437
45. Wang G, Kwan BC, Lai FM, et al. Intrarenal expression of miRNAs in patients with hypertensive nephrosclerosis. Am J Hypertens 2010;23:78–84
46. Wang G, Kwan BC, Lai FM, et al. Intrarenal expression of microRNAs in patients with IgA nephropathy. Lab Invest 2010;90:98–103